Asian Journal of Chemistry; Vol. 27, No. 3 (2015), 1056-1062

ASIAN JOURNAL OF CHEMISTRY

http://dx.doi.org/10.14233/ajchem.2015.18225

Carbonaceous Materials-Based Electric Double Layer Capacitors with Improved Electrochemical Performance

LEI ZHU[1], ASGHAR ALI[1], SHU YE[1], KEFAYAT ULLA[1], CHANG-ZHOU YUAN[3], ICK-JUN KIM[2], SUN-HYE YANG[2] and WON-CHUN OH[1,*]

[1]Department of Advanced Materials Science & Engineering, Hanseo University, Seosan-si, Chungnam 356-706, Republic of Korea
[2]Korea Electrotechnology Research Institute, Changwon-si, Kyungnam 641-120, Republic of Korea
[3]Institute of Energy Storage Materials and Devices, Department of Science and Engineering, Anhui University of Technology, Maanshan 243002, P.R. China

*Corresponding author: Fax: +82 41 6883352; Tel: +82 41 6601337; E-mail: wc_oh@hanseo.ac.kr

Received: 31 May 2014; *Accepted*: 6 August 2014; *Published online*: 19 January 2015; AJC-16724

In this study, the fabrication of working electrodes was carried out as follows. Briefly, the electrodes were composed of graphene as an active material, Ketjen black and activated carbon fiber as an electric conductor and polytetrafluoroethylene [$(C_2F_4)n$, PTFE] as a binder. The prepared electrodes were characterized by X-ray diffraction and scanning electron microscopy. Finally, the electrochemical performances of carbon materials in the electrolyte solution of tetraethylammonium tetrafluoroborate [$(C_2H_5)_4NBF_4$, $TEABF_4$] in propylene carbonate were examined. The graphene nanosheets electrode in the work exhibited a good rate of capability and reversibility at high scan rates in electrochemical performances.

Keywords: Graphene, Kezjen black, Electrochemical double-layer, X-ray diffraction, Electrochemical performance.

INTRODUCTION

Supercapacitors are becoming more and more popular because they can improve the performance of electrolytic capacitors in terms of specific energy and that of rechargeable batteries in terms of specific power. In addition, supercapacitors have a much longer cycle life than batteries because there are no or negligibly small chemical charge transfer reactions involved[1,2].

Within the last years, a number of studies were dedicated to improve the performance of supercapacitors by developing new types of carbon materials *e.g.*, carbon nanotubes, carbon nanofibers, carbon aerogel, carbon xerogel and glassy carbon. However, due to their low cost and expected good cycleability, activated carbon-based supercapacitors remain as the lonely practical candidates for industrial applications, particulalry for electric vehicles and power quality devices[3]. The supercapacitor establishes capacitance *via* the electrochemical double-layer Both the supercapacitors and batteries are critical energy/power storage devices for portable electronics, wind power and electrical vehicles[4]. The development of the electrical vehicles industry primarily relies on the advancement of long-life, fast-charging and large-capacity batteries. However, the battery and the supercapacitor are not mutually replaceable and have distinct roles in the electrical vehicles's power-train system. The battery relies on chemical reaction and electrolyte ion diffusion in order to generate/store energy. Moreover, it can deliver much more energy than the supercapacitor[5]. On the other hand, a supercapacitor depends on the electrochemical double-layer in order to store/release energy. Further, it can be rapidly charged and discharged by avoiding chemical reactions in devices. The supercapacitor can endure repeated cycles for many years without degradation and contains no heavy ions in the electrolyte/electrode, making it an environmentally friendly device[6].

Carbonaceous materials are widely used for supercapacitor electrodes due to their relatively low cost, versatile existing forms, large specific surface area, good electric conductivity and excellent chemical stability[7]. Generally, the highly developed surface area and porosity are necessary for carbon electrodes to obtain high specific capacitance. Hence, activated carbons have been widely adopted as electrode materials for the supercapacitor[8].

Carbon allotropes are used as conductive additives because they have a large surface to volume ratio, high liquid absorbance and high electrical conductivity[9]. The main roles of carbon additives are to increase the contact points between the cathode-active material and the current collector and to serve as the joints in order to form a continuous network among the active material particles. Furthermore, the carbon additives

can absorb and retain the electrolyte, resulting in a better contact of the electrolyte with the active material as well. However, the carbon additives also have some negative effects for Li^+ batteries. In particular, in case of a large amount of addition, it may lead to a decrease of battery power and/or the formation of an inhomogeneous distribution, causing a polarization in the electrode. To overcome this problem, we attempted to use a specific form of carbon black, *i.e*., Ketjen black EC-600 J, as the cathode additive due to its large specific surface area (about 1270 m^2g^{-1}), which may reduce the usage of the carbon additive while retaining equally good properties of the heavily doped graphene electrode. However, there is a tendency for large Ketjen black flakes to overlay and form thick stacks, hence, eliminating the advantage of Ketjen black[10,11].

Graphene is a two-dimensional carbon plane with one-atomic thickness; it emerges as a unique morphology carbon material with the potential for electrochemical energy storage device applications due to its chemical stability, high electrical conductivity and large surface area[12]. Compared to other carbon materials, graphene has an ultra-low resistivity for electron transport. At room temperature, the resistivity of the graphene sheet is -10^{-6} Ω cm (less than the resistivity of silver). The specific area of a single graphene sheet could approach 2630 m^2g^{-1}. A research, led by Schindall for the MIT LEES project, has demonstrated supercapacitors with 30 Wh kg^{-1}. Studies of the graphene-based supercapacitor, led by Ruoff and co-workers[5] reported that chemically modified graphene could gain very high specific capacitance (137 F g^{-1}) in an aqueous solution. Hence, these properties suggest wide applications, including field effect transistors, adsorbents, lithium-ion batteries and supercapacitors.

The purpose of this paper is to understand the effect on the electrochemical capacitance of three commercial carbon materials, graphene, Ketjen black and activated carbon fiber. We prepared the resultant electrode with kneading type. The prepared samples were characterized by X-ray diffraction and a scanning electron microscopy analysis, Finally, the electrochemical performances of graphene nanosheets in an electrolyte solution of tetraethylammonium tetrafluoroborate [$(C_2H_5)_4NBF_4$, TEABF$_4$] in propylene carbonate ($C_4H_6O_3$, PC) were examined.

EXPERIMENTAL

Synthesis of graphene: For graphene synthesis, graphene oxide was prepared and then, graphene was obtained after the reduction of graphene oxide using a reduction agent. First, graphite (KS-6) was selected as the starting material. Subsequently, graphene oxide was prepared from graphite according to the Hummers-Offeman method[13]. In brief, graphite powder (10 g) was dispersed in cold conc. sulphuric acid (230 mL, 98 wt % and dry ice bath) and potassium permanganate (30 g) was gradually added with continuous vigorous stirring and cooling in order to prevent the temperature from exceeding 293 K. The dry ice bath was removed and replaced by a water bath. Then, the mixture was heated to 308 K for 0.5 h under continuous stirring, followed by a slow addition of deionized water (460 mL), which produced a rapid increase in the solution temperature up to a maximum of 371 K. The reaction was maintained for 40 min in order to increase the oxidation degree of the graphite oxide product. With the addition of more distilled water (140 mL), followed by the addition of hydrogen peroxide solution (30 %, 30 mL), the resultant bright-yellow suspension was terminated. The solid product was separated by centrifugation at 3000 rpm and washed initially with 5 % HCl until sulphate ions were no longer detectable with barium chloride. Then, it was washed three times with acetone and air dried overnight at 338 K. After sonication for 30 min, the graphite oxide was translated to graphene oxide.

The reduction of graphene oxide was performed as follows: 25 mg of graphene oxide powder was placed in a cup and 200 mL de-ionized water was added. Ten minutes of magnetic stirring at 200 rpm yielded an inhomogeneous brown suspension.

The resulting suspensions were further treated with a reduction agent hydrazine solution (1:5, volume ratio of hydrazine to deionized water) under ultrasonication (0.5 h, 1.3 × 105 J); after drying at 373 K, the sample reduced from the graphene oxide was simply graphene.

Sample characterization: X-ray diffraction (Shimadzu XD-D1, Uki, Kumamoto, Japan) was used to identify the crystallinity of the composite with monochromatic high-intensity CuK_α radiation (λ = 1.5406 Å). SEM (JSM-5600, JEOL Ltd., Tokyo, Japan) was used to observe the surface state and structure of the prepared composite.

Preparation of electrochemical double-layer electrode: The fabrication of working electrodes was carried out as follows. Briefly, the electrodes were composed of graphene as an active material, Ketjen black and activated carbon fiber as an electric conductor and polytetrafluoroethylene as a binder. The weight ratio of the active material, electric conductor and binder was 85:5:10 wt %. The components of the electrode were mixed at 3000 rpm in the solvent in order to make slurry. Then, the cells were assembled with an electrolyte impregnated in the separator sandwiched between the electrodes, whose size was 2 cm × 2 cm. These assemblages were housed in Al-laminated film cells. After each organic electrolyte solution of 1.8 mtetraethylammonium tetrafluoroborate [$(C_2H_5)_4NBF_4$, TEABF$_4$] in propylene carbonate ($C_4H_6O_3$), respectively, was poured, the cells were sealed, taking out the leads. Fig. 1 describes the cell used for electrochemical measurements. Nomenclatures and prepare method for samples (SH1, SH2, SH3, SM1, SM2, SM3) was listed in Table-1.

Electrochemical performance of electrochemical double-layer electrode: The cyclic voltamogram of electrodes were measured between the voltage ranges of 0-2.5 V at different potential scan rates of 1, 3, 5 and 10 mV/s. For the charge/

TABLE-1
NOMENCLATURES AND PREPARE METHOD FOR SAMPLES

Nomenclatures	Graphene (%)	Ketjen black (%)	Activated carbon fiber (%)	BET (m^2/g)
SH1	20	10	70	932.7
SH2	20	20	60	823.8
SH3	20	30	50	820.1
SM1	20	10	70	833.5
SM2	20	20	60	754.1
SM3	20	30	50	733.2

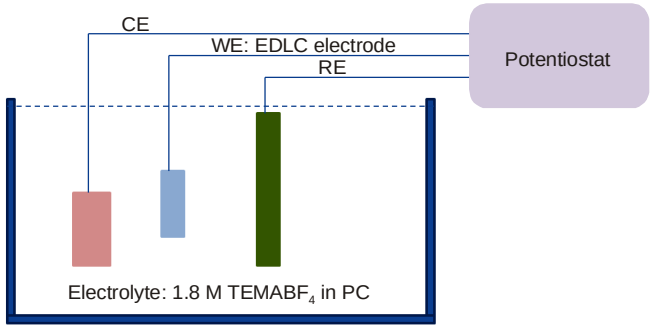

Fig. 1. Schematic illustration of cyclic voltammetry experimental apparatus, (CE = counter electrode and RE = reference electrode)

discharge experiment, the cells were charged and discharged using the galvanostatic method tested by two paths, (a) 3 cycles at 0-2.5 V and (b) first cycle at 0-4 V, second and third cycles at 0-2.5 V. It was then measured under a current density of 2 mA/cm^2.

RESULTS AND DISCUSSION

Microstructure characterizations: The micro-surface structures and morphologies of the composites were characterized by SEM (Fig. 2). The SEM technique is used for inspecting topographies of specimens at very high magnifications, using a piece of equipment called the scanning electron microscope. Fig. 1 indicates the macroscopic changes in the morphology of the composites. In Fig. 2a is SH1, Fig. 2b is SH3, Fig. 2c is SM1 and Fig. 2d is SM3. In addition, all of the carbon particles have a small particle size and a good dispersion in Fig. 2. Thus, we conjecture that the banding particles in the composites are activated carbon fiber particles. SH1 has more activated carbon fiber particles than SH3. Overall, we can find activated carbon fiber particles from all of the samples. By comparing with Fig. 2a,b, after increasing the content of activated carbon fiber, the dispersion of carbon materials has slightly deteriorated. We can also find some flake particles here as well. Hence, we conjecture that these flake particles in the sample are graphene.

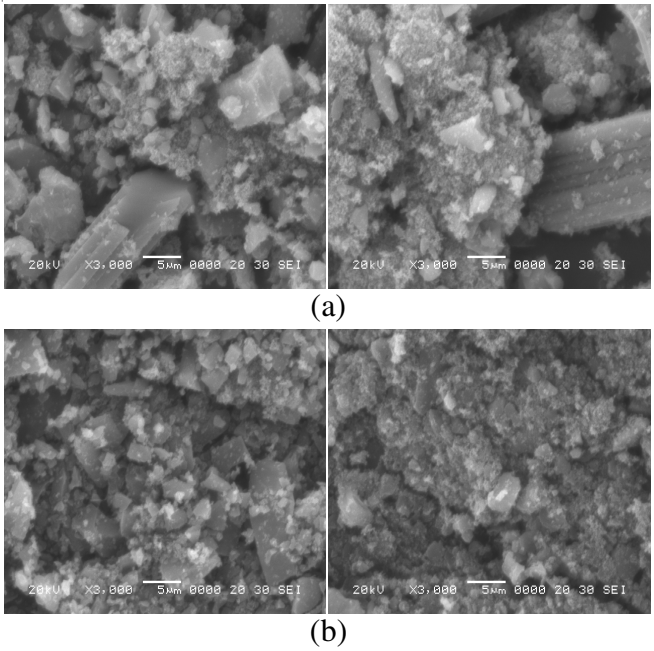

Fig. 2. SEM microphotograph of samples

X-ray diffraction was used to determine the crystallographic structure of the inorganic component of the composite. X-ray diffraction patterns of the prepared graphene nanosheets are shown in Fig. 3. The diffraction peaks at 2θ = 26° and 43° can be attributed to the graphite-like structure (002) and (100) (JCPDS No. 01-0646)[14,15], respectively. The broad peak at 26° corresponding to a d-spacing of 3.413 Å can also be obtained. From the XRD patterns (Fig. 4), it is also possible to compute the % crystallinity and crystallite size. The amorphous phase fraction of the sample may be determined by taking the ratio of the amorphous area (area not under the peaks) of the X-ray diffractogram to the total area.

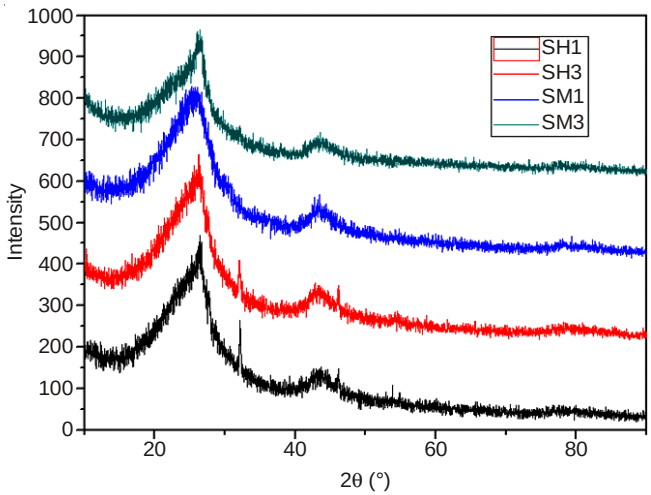

Fig. 3. Typical XRD pattern of prepared electrodes

The surface area of carbonaceous materials with various graphene and activated carbon fiber ratios along with fixed kitchen black was calculated by using the Brunauer, Emmett and Teller (BET) method[16]. The simple illustration of the process as, after cooling the sample nitrogen gas was blown, thus the surface absorb the gas molecules. By increasing the amount of gas the multilayer surface will absorb more molecules to cover the whole surface of the sample. The absorbability depends on the pressure of the gas. Because our samples are a multilayer, it is very difficult to precisely determine the amount of a single layer molecule. However, according to the reports, during the process of one layer to multilayer, the adsorption value of the single-layer molecule can be calculated precisely by the "expression of BET." The surface areas of all samples are collected in Table-2. SH1 has the biggest surface area, higher than any other samples. Having a good surface area can lead to good electrochemical performances. We compare the electrochemical performance of different samples in order to research their electrochemical ability.

Electrochemical performances: The specific capacitance of the graphene electrode can be calculated according to the following equation:

$$C = \frac{\left(\int IdV\right)}{\nu m V}$$

where I is the response current density (A cm^{-2}), V is the potential (V), ν is the potential scan rate (mVs^{-1}) and m is the

TABLE-2
SPECIFIC CAPACITANCE OF DIFFERENT ELECTRODES

Sample		Capacity (mAh)	Capacitance (F)	Sp. capacitance (F/g)	Sp. capacitance (F/cc)	Electrode density (g/cc)
SM1	Path 1	1.1	1.6	13.6	8.5	0.7343
	Path 2	2.58	2.3	19.9	12.4	0.7343
SM3	Path 1	0.7	1.0	11.4	5.3	0.5460
	Path 2	1.89	1.3	13.6	6.7	0.5460
SH1	Path 1	0.9	1.3	12.8	7.1	0.6531
	Path 2	2.61	2.4	22.4	12.4	0.6531
SH3	Path 1	0.9	1.3	13.6	6.7	0.5850
	Path 2	2.40	2.2	22.9	11.4	0.5850

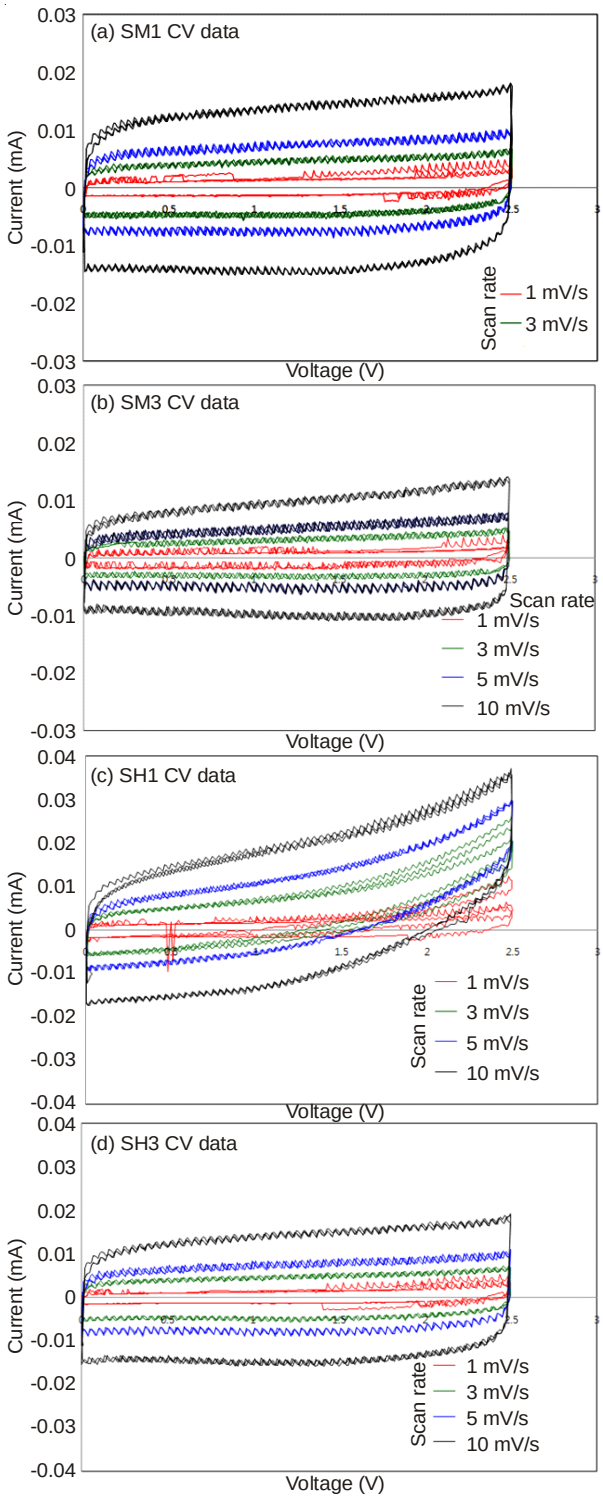

Fig. 4. Cyclic voltammetry curves of electrode at different scan rates of 1, 3, 5 and 10 mVs^{-1}

mass of the graphene nanosheets in the electrode (g). Cyclic voltammetry measurements were carried out within the potential range of 0-2.5 V in order to analyze the electrochemical behaviour of the graphene electrode. Fig. 4 shows the cyclic voltammetry curves of graphene electrode at scan rates varying from 1 to 10 mVs^{-1}. In Fig. 4, (a) is SM1, (b) is SM3, (c) is SH1 and (d) is SH3 are shown.

The typical rectangular curve without the obvious oxygen and hydrogen evolution peaks can be observed at all scan rates, indicating good charge propagation within the electrode. It can be also noted that the cathodic peaks shift positively, whereas the anodic peaks shift negatively with the increment of potential sweep rates from 1 to 10 mVs^{-1}, which is primarily due to the resistance of the electrode[17]. In addition, the obvious increase in the current scan rates implies a good rate capability.

At the identical scan rate, the most ideal capacitive behaviour was observed for SH1, with the steepest current change at the switching potential (0 to 1.0 V) observing the most rectangular shape of the I-V curves. The faster change at the switching potentials in the cyclic voltammetry plot of SH1 than SH2 and SH3 stem from the faster reformation of the double layer in SH1, most likely due to the faster ionic motions in its micropores. In addition, higher capacitance was obtained from SH1 than SH2 and SH3, signifying that more surface area of the carbon was accessed by the electrolyte ions. This result suggests a more reasonable pore distribution and surface area of the SH1, which is also in agreement with the above results[18].

Cyclic voltammetry was performed for the electrode made from various graphene and activated carbon fiber ratios with fixed kitchen black samples. The representative cyclic voltammograms in 3 M KOH electrolyte at the potential scan rate of 1 mV/S are shown in Fig. 4. A slightly distorted and symmetric rectangular shape was observed for all samples, which implies that a double-layer formation in 3 M KOH electrolyte and a generation of equivalent series resistance (ESR) occurred in all samples. From the plot, it is clear that the sample with 20 wt % of graphene has the large capacitance with smaller Rct, showing enhanced conductivity due to graphene. The specific capacitance of the entire sample decreased by increasing the weight ratio of activated carbon fiber, thus decreasing the kitchen black values with fixed additive conductive graphene. This result was related to the instability of double-layer formation ensuing from lowered accessibility of ions with the exposed pore surface. The details properties of the electrochemical double-layer electrodes are provided in Table-2.

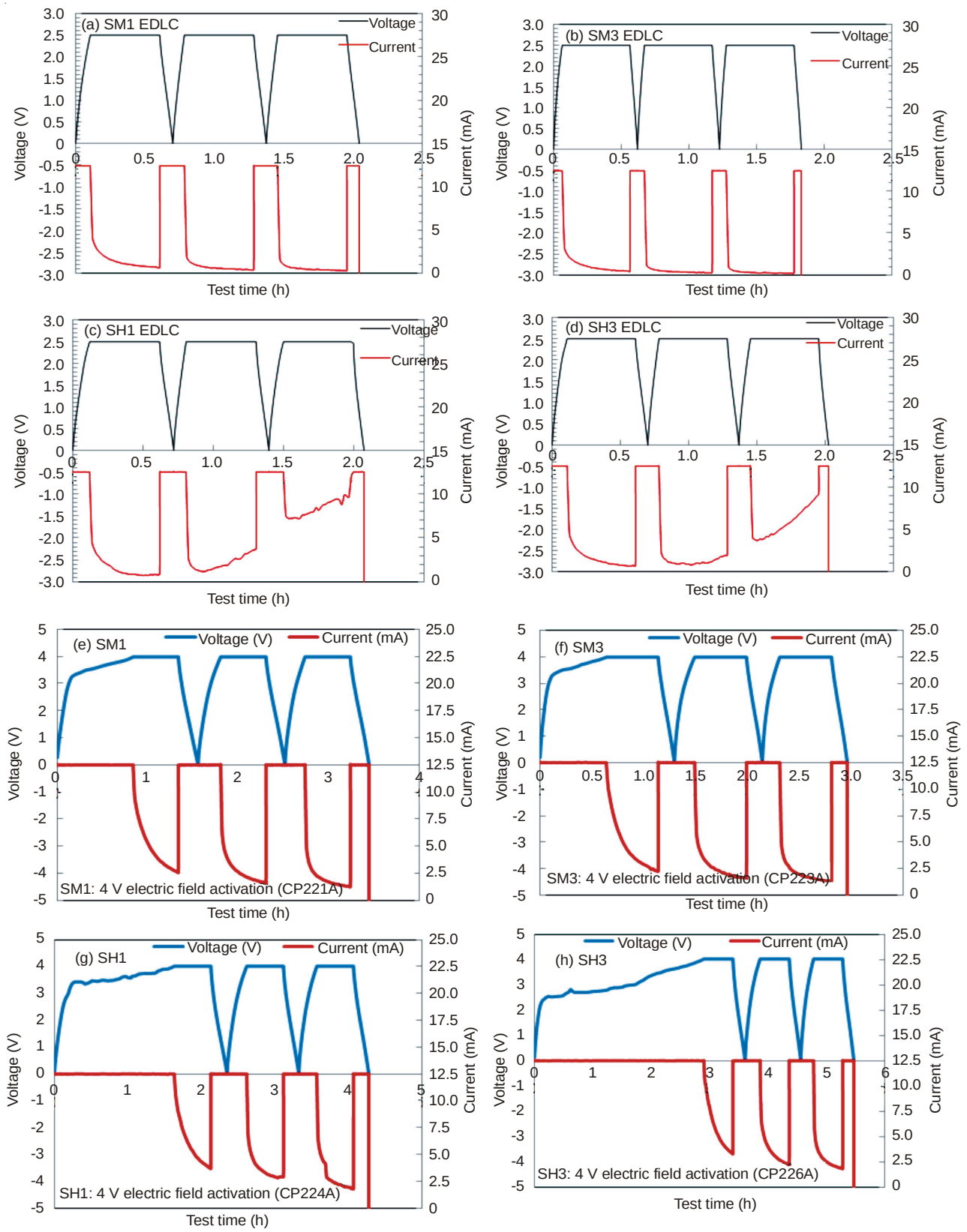

Fig. 5. Galvanostatic charge/discharge teats of graphene electrode at current density of 2 mA/cm^2 tested by two paths; (a) 3 cycles at 0-2.5 V; (b) first cycle at 0-4 V and second and third cycles at 0-2.5 V

To investigate the electrochemical performance of prepared graphene nanosheets as the electrode for electrochemical double-layer, galvanostatic charge/discharge cycling measurements were performed. Fig. 5 shows the galvanostatic charge/discharge cycling curves at the current density of 2 mA/cm^2 tested by two paths, path 1 (a-d) 3 cycles at 0-2.5 V and path 2 (e-h) first cycle at 0-4 V and the second and third cycles at 0-2.5 V. For path 1, after 3 cycles at 0-2.5 V, the well-retained

rectangular-shaped curve appears in Fig. 5. However, for path (e-h), after the first cycle at 0-4 V, there are two clear voltage stages included in the curves: 0-3.1 and 3.1-4 V, respectively. During the former, short charge/discharge duration is ascribed purely to the electric double-layer capacitance of the electrode. During the latter, the combination of electric double-layer capacitance and Faradaic capacitance is responsible for the longer charge/discharge duration due to the faradaic charge-transfer. Moreover, after the first cycle at 0-4 V, the second and third cycles at 0-2.5 V were also performed. Compared to path (a), the charge/discharge duration at the second and third cycles at 0-2.5 V is increased by almost 2 times, indicating that the capacitance is larger.

The specific capacitances of the prepared electrode are summarized in Table-2. The specific capacitances per weight and volume increase with the increase in the number of cycles in both paths 1 and 2. At the same voltage of 0-2.5 V, in the second and third cycles, the specific capacitances per weight and volume in path 2 is much larger than that in path 1, which reached 19.9 F/g and 12.4 F/cc of SM1, 22.4 F/g and 12.4 F/CC of SH1, respectively. From Table-2, the capacitances of the samples were increased with the increased content of activated carbon fiber. Changing the value of the content leads to various specific capacitances. As in SM3 and SH3, the Ketjen black content was increased from 10 to 30 wt % thereby decreasing the capacitance, which may be due to the decrease in the activated carbon fiber value in the sample with a maximum value of graphene. Further, this result may be due to the agglomeration of the graphene sheet on the surface of activated carbon fiber to lower the surface area and thus, providing a small amount of the conductive additive value to react with the activated carbon surfaces. This effect is consistent with the results of the BET surface area test, which is explained previously.

Electrochemical impedance spectroscopy (EIS) as a powerful technique was further employed to monitor the electrochemical behaviours of electrodes. Impedance spectra for the electrode after the first cycle at 0-2.5 and 0-4 V are presented in Fig. 6, where the real part (Z') corresponds to the equivalent of ohmic resistance and the imaginary part (Z") reflects the presence of non-resistive elements[19]. Nyquist impedance plots for the sample electrodes were tested (a, b) after first cycle at 0-2.5 V and (c, d) after first cycle at 0-4 V. The impedance behaviour might be dominated by three major processes occurring in the high, medium and low frequency regions, respectively[20,21]. The radius of the semicircle in the high frequency region reflects the impedance on the electrode/electrolyte interface. The slope of the 45° portion of the curve in the medium frequency region is referred to as the Warburg resistance and is a result of the frequency-dependent of ion diffusion/transport in the electrolyte. By comparing the patterns in Fig. 6, the radius of the semicircle in the electrode tested after the first cycle at 0-4 V is the largest, indicating that polarization resistance is high. In addition, the electrode tested after the first cycle at 0-4 V shows a large Warburg region, which may be due to the closed surface of the prepared electrode with few edges. Ion diffusion into the interior of the agglomerate would result in greater variations in the ion diffusion path lengths as well as an increased obstruction of ion

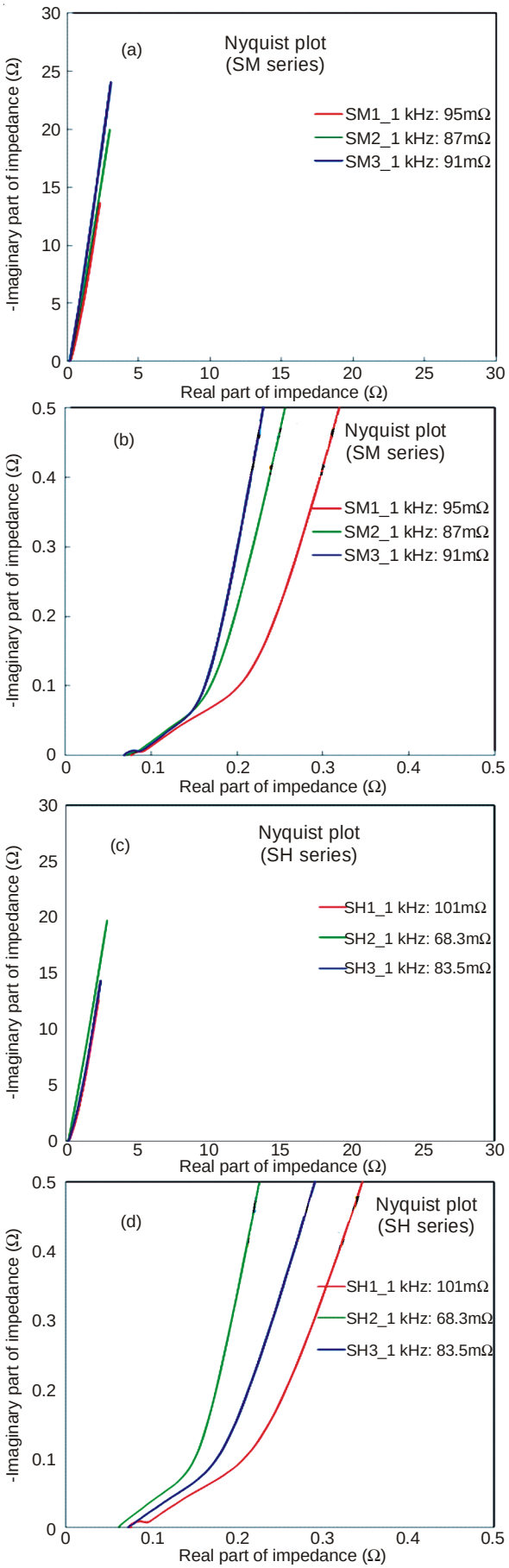

Fig. 6. Nyquist impedance plots for sample electrodes tested (a, b) after first cycle at 0-2.5 V and (c, d) after first cycle at 0-4 V

movement, leading to a large Warburg region[7]. On the other hand, the impedance spectrum of the electrode tested after the first cycle at 0-2.5 V displays a vertical line close to 90° at low frequency, which indicates a purely capacitive behaviour. The internal resistance at 1 kHz for the electrode tested in paths 1 and 2 is estimated to be 0.44 Ω and 2.71 Ω, respectively. The supercapacitor exhibits an ideal capacitor behaviour due to the fast doping/dedoping rates during the redox reactions. The doping/dedoping process involves the charge (electrons or holes) transport with ions transport in the supercapacitor. Here, the ion transport rate determines the charge/discharge rate of graphene nanosheets due to the slow charge transport in the supercapacitor. Further, the electrode presents a phase angle close to 90° in a high, low frequency region, following the trend of ideal capacitive behaviour and agrees with the cyclic voltammetry results[22-24]. Different samples have different resistance, as shown in Table-2. SM 3 has a smaller resistance, because the content of Ketjen black is higher than SM1. From Table-2, which conveys various graphene and activated carbon fiber ratios with fixed kitchen black of samples, we can note that the resistance was decreased with the increased content of Ketjen black.

It is expected that the electrode with high electrical conductivity would have improved high rate capability[25]. Therefore, we studied the rate capability of the different electrodes at different rates. Fig. 7 shows the variation in the capacity retention at different rates for the electrodes. Fig. 7a is the capacity retention for SM1, SM2 and SM3. Fig. 7b is the capacity retention for SH1, SH2 and SH3. The rate of performance was determined after 3 cycles by using the charge and discharge

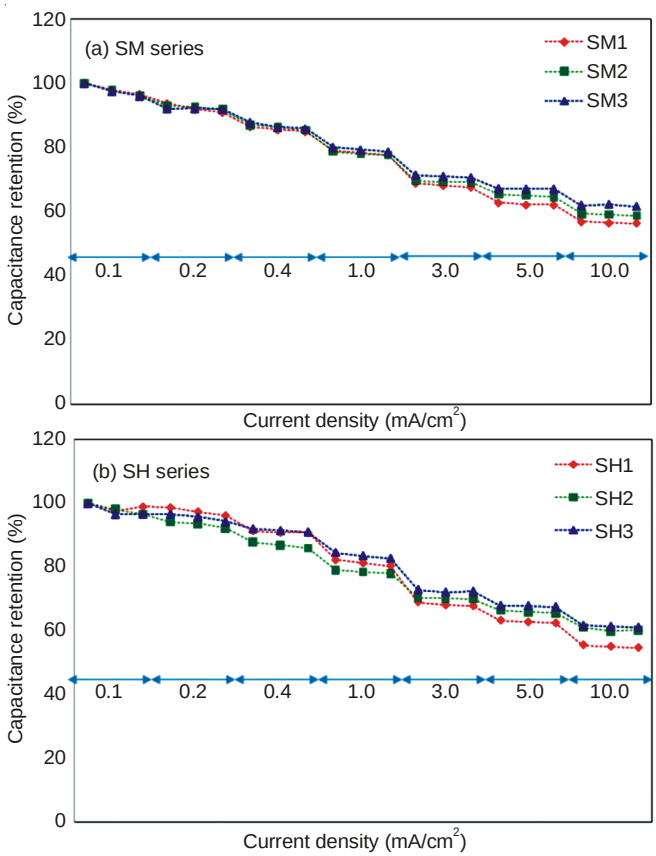

Fig. 7. Rate performance of different electrodes

current of 0.1 mA/cm^{-1} and 0.1 (0.2, 0.4.....10) mA/cm^{-1}, respectively. At a low rate of 0.1 and 0.2 mA/cm^{-1}, the capacitance is about 3.8 F/g. The capacitances decrease with increases in the amount of the discharge current.

Conclusion

In this study, we have investigated the electrochemical performance of graphene nanosheets as electrode materials for electrochemical double-layer. The graphene nanosheets electrode in present experiment exhibited a good rate of capability and reversibility at high scan rates in electrochemical performances. At the same voltage of 0-2.5 V in the second and third cycles, the specific capacitances per weight and volume in path 2 are much larger than that in path 1, which reached 19.9 F/g and 12.4 F/cc of SM1, 22.4 F/g and 12.4 F/CC of SH1, respectively. The internal resistance at 1 kHz for the electrochemical double-layer tested in path 1 and 2 is estimated to be 0.44 Ω and 2.71 Ω, respectively. Hence, SM1 and SH1 have good capacitor ability. However, the resistance was decreased with the increased content of Ketjen black.

ACKNOWLEDGEMENTS

This work was supported by the Next Generation Secondary Battery R&D Program of MOTIE/KEIT. [10042575, Development of 5kW Zn-air battery for EV and 3.3V-1,000F pouch type high-power supercapacitor].

REFERENCES

1. A. Burke, *J. Power Sources*, **91**, 37 (2000).
2. M. Winter and R.J. Brodd, *Chem. Rev.*, **104**, 4245 (2004).
3. B.E. Conway, Electrochemical Supercapacitors: Scientific Fundamentals and Technological Applications, Kluwer Academic/Plenum Publishers, New York, edn. 1 (1999).
4. C. Ashtiani, R. Wright and G. Hunt, *J. Power Sources*, **154**, 561 (2006).
5. M.D. Stoller, S. Park, Y. Zhu, J. An and R.S. Ruoff, *Nano Lett.*, **8**, 3498 (2008).
6. A.K. Geim and K.S. Novoselov, *Nat. Mater.*, **6**, 183 (2007).
7. J.C. Meyer, A.K. Geim, M.I. Katsnelson, K.S. Novoselov, T.J. Booth and S. Roth, *Nature*, **446**, 60 (2007).
8. A.K. Geim and K.S. Novoselov, *Nat. Mater.*, **6**, 183 (2007).
9. D.A. Areshkin, D. Gunlycke and C.T. White, *Nano Lett.*, **7**, 204 (2007).
10. J. Schindall, *IEEE Power Electron. Soc. Newslett.*, **20**, 32 (2007).
11. J. Schindall, The Charge of the Ultra-Capacitors, IEEE Spectrum. IEEE (2007); http://www.spectrum.ieee.org/nov07/5636.
12. S. Stankovich, D.A. Dikin, R.D. Piner, K.A. Kohlhaas, A. Kleinhammes, Y. Jia, Y. Wu, S.T. Nguyen and R.S. Ruoff, *Carbon*, **45**, 1558 (2007).
13. W.C. Oh and F.J. Zhang, *Asian J. Chem.*, **23**, 875 (2011).
14. K. Gotoh, T. Kinumoto, E. Fujii, A. Yamamoto, H. Hashimoto, T. Ohkubo, A. Itadani, Y. Kuroda and H. Ishida, *Carbon*, **49**, 1118 (2011).
15. W.C. Oh, F.J. Zhang and M.L. Chen, *J. Ind. Eng. Chem.*, **16**, 321 (2010).
16. Y.G. Wang, H.Q. Li and Y.Y. Xia, *Adv. Mater.*, **18**, 2619 (2006).
17. B. Fang, Y.Z. Wei, K. Suzuki and M. Kumagai, *Electrochim. Acta*, **50**, 3616 (2005).
18. X.H. Xia, L. Shi, H.B. Liu, L. Yang and Y.D. He, *J. Phys. Chem. Solids*, **73**, 385 (2012).
19. L. Li, H. Song and X. Chen, *Electrochim. Acta*, **51**, 5715 (2006).
20. F. Li, J. Song, H. Yang, S. Gan, Q. Zhang, D. Han, A. Ivaska and L. Niu, *Nanotechnology*, **20**, 455602 (2009).
21. H. Li, H. Xi, S. Zhu, Z. Wen and R. Wang, *Microporous Mesoporous Mater.*, **96**, 357 (2006).
22. J.H. Han, K.W. Cho, K.H. Lee and H. Kim, *Carbon*, **36**, 1801 (1998).
23. A.C. Ferrari and J. Robertson, *Phys. Rev. B*, **61**, 14095 (2000).
24. L.G. Cancado, M.A. Pimenta, B.R.A. Neves, M.S.S. Dantas and A. Jorio, *Phys. Rev. Lett.*, **93**, 247401 (2004).
25. M.L. Chen, C.Y. Park, Z.D. Meng, L. Zhu, J.G. Choi, T. Ghosh, L.J. Kim, S. Yang, M.K. Bae, F.J. Zhang and W.C. Oh, *Fullerenes, Nanotubes, Carbon Nanostruct.*, **21**, 525 (2013).